Observation of positive and negative magneto-LC effects in all-organic nitroxide radical liquid crystals by EPR spectroscopy

Katsuaki Suzuki, Yoshiaki Uchida, Rui Tamura, Satoshi Shimono and Jun Yamauchi*

Graduate School of Human and Environmental Studies, Kyoto University, Kyoto 606-8501, Japan

Electronic Supplementary Information

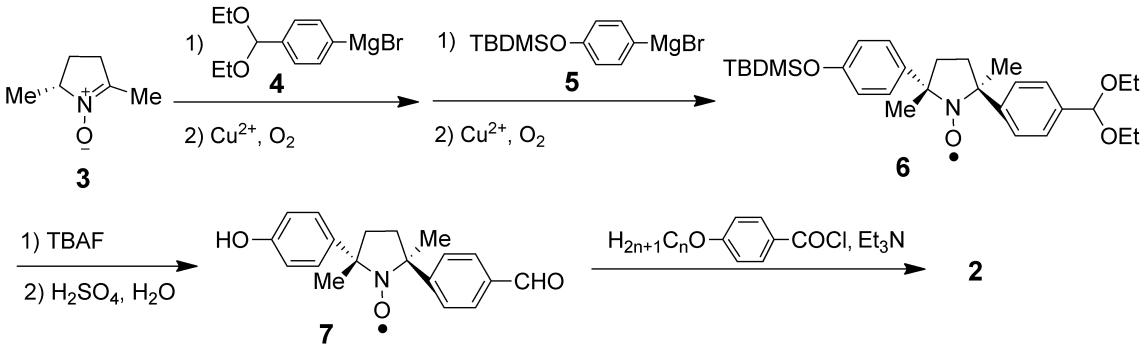

Scheme S1. Preparation of **2**.

Preparation of 2

(2*S*,5*S*)-2-[4-(*tert*-Butyldimethylsiloxy)phenyl]-5-[4-(diethoxymethyl)phenyl]-2,5-dimethyl pyrrolidine-1-oxy (6): Chiral nitrone (*R*)-**3** was prepared according to the published procedure[S1)]. To a stirred solution of the freshly prepared Grinard reagent **4** (10 mmol) in THF (10 mL) was slowly added a solution of the nitrone (*R*)-**3** (0.565 g, 5.0 mmol) in THF (10 mL) under argon at –78°C. The temperature was raised slowly to 25°C, and stirring was continued overnight. The reaction mixture was poured into saturated aqueous NH_4Cl solution (50 mL), and then extracted with ether (2 × 50 mL). The combined ether extract was dried over $MgSO_4$ and evaporated. The residual oil was dissolved in methanol (20mL). To this solution were added 25% aqueous NH_3 solution (1.4 mL) and copper (II) acetate monohydrate (0.160 g, 0.80 mmol). Oxygen was bubbled through the yellow solution until a persistent deep blue color developed. The solvent was then removed under reduced pressure and the crude product was dissolved in dichloromethane (DCM) (50 mL). This solution was washed with saturated aqueous $NaHCO_3$ solution (50 mL), dried over $MgSO_4$, and evaporated. The water was removed by azeotropic method with benzene

and the remaining trace of benzene was removed in vacuo. The crude product was dissolved in THF (10 mL) and reacted with freshly prepared Grinard reagent **5** (the same quantity and conditions as described above). After a similar workup procedure, the crude product **6** (24% yield) was obtained by short column chromatography on silica gel (hexane/ether 9:1).

S1 J. Einhorn, C. Einhorn, F. Ratajczak, I. Gautier-Luneau, J. L. Pierre, *J. Org. Chem*., 1997, **62**, 9385–9388.

(2*S*,5*S*)-2-(4-Hydroxyphenyl)-5-(4-formylphenyl)-2,5-dimethylpyrrolidine-1-oxy (7): To (2*S*,5*S*)-**6** (0.199 g, 0.40 mmol) dissolved in THF (10 mL) was added 0.5mL of tetrabutylammonium fluoride (1M solution in THF) at 0°C. After stirring for 1 h, the reaction mixture was poured into saturated aqueous NH_4Cl solution (20 mL), and the aqueous phase was extracted with ether (3 x 30 mL). The combined organic phase was dried over $MgSO_4$ and concentrated in vacuo. Flash column chromatography on silica gel (DCM/ether 8:2~7:3) of the residue gave yellow oil. To a solution of the yellow oil in THF (2 mL) was added 5% aqueous H_2SO_4 solution (3 mL) and the mixture was stirred for 30min at room temperature. Brine and DCM were then added. The organic phase was separated, dried over $MgSO_4$, and evaporated. Flash column chromatography on silica gel (DCM/ether 8:2~7:3) of the residue gave yellow solid. The crude product was recrystallized from hexane/ether (8:2) to give pure (2*S*,5*S*)-**7** in 61% yield. (2*S*,5*S*)-**7**: EPR (THF): g = 2.0066, a_N = 1.32 mT. IR (KBr) 3339, 2981, 2948, 2241, 1938, 1892, 1825, 1705, 1513, 1457, 1412, 1371, 1315, 1256, 1179, 1111, 1069, 840 cm^{-1}. Anal. Calcd for $C_{19}H_{20}NO_3$: C, 73.53; H, 6.50; N, 4.51; Found: C, 73.35; H, 6.52; N, 4.43.

(2*S*,5*S*)-2-[4-(4-Alkoxybenzenecarbonyloxy)phenyl]-5-(4-formylphenyl)-2,5-dimethylpyrrolidine-1-oxy (2): To (2*S*,5*S*)-**7** (0.031 g, 0.10 mmol) dissolved in THF (3 mL) was added Et_3N (0.50 mL, 0.69 mmol) and 4-alkoxybenzoyl chloride (0.3 mmol) dissolved in THF (3 mL) at 0°C. The reaction mixture was slowly warmed to 25°C. After 40h, the mixture was poured into saturated aqueous $NaHCO_3$ solution (30 mL) and extracted with ether (3 × 50 mL). The combined organic phase was dried over $MgSO_4$ and evaporated. Flash column chromatography on silica gel (hexane/DCM/ether 7:2:1) of the residue gave pure **2** as yellow solid. The *ee* values of **2** were determined by HPLC analysis (Fig. S1, ESI†).

(2*S*,5*S*)-**2a** (n=10) (96% *ee*) (84% yield from **7**): $[\alpha]_D^{20}$ –126° (c 0.593, THF). EPR (THF): g=2.0059, a_N =1.33 mT. IR (KBr): 2922, 2850, 1730, 1691, 1605, 1506, 1258, 1206, 1071, 1015,

847, 766, 723 cm^{-1}. Anal. Calcd for $C_{36}H_{44}NO_5$: C, 75.76; H, 7.77; N, 2.45; Found: C, 75.85; H, 7.80; N, 2.44.

(2*S*,5*S*)-**2b** (n=18) (89% *ee*) (78% yield from **7**): $[\alpha]_D^{20}$ –108° (c 0.541, THF). EPR (THF): g=2.0059, a_N = 1.33 mT. IR (KBr): 2920, 2850, 1734, 1701, 1604, 1508, 1450, 1252, 1167, 1071, 1008, 845, 763, 725 cm^{-1}. Anal. Calcd for $C_{44}H_{60}NO_5$: C, 77.38; H, 8.86; N, 2.05; Found: C, 77.30; H, 8.87; N, 2.14.

Table S1. Magnetic Properties and Phase Transition Behavior of **2**.

	EPR[a]		SQUID[b]		Phase transition temperature[c] (°C)
	ee (%)	g	a_N (mT)	C (emu K mol^{-1})[d]	θ(K)[e]	(transition enthalpy[c] (kJ/mol))
2a	0	2.0059	1.33	0.38	-7.30	K 103.4 (41.4) N 108.6 (1.05) Iso : heating
						Iso 106.7 (1.57) N 39.7 (14.1) K : cooling
	96			0.36	-0.54	K 75.2 (15.1) N* 106.0 (1.2) Iso : heating
						Iso 104.4 (1.3) N*[f] : cooling
2b	0	2.0059	1.33	0.38	-1.04	K 107.3 (56.5) Iso : heating
						Iso 98.3 (2.4) SmA 75.8 (46.4) K : cooling
	87			0.36	-1.16	K 76.7 (9.83) K 87.7 (42.4) SmA* 104.6 (4.97) Iso : heating
						Iso 101.4 (3.1) SmA* 62.1 (33.0) K : cooling

[a]Measured in THF at 25°C. [b]Measured in a temperature range of 2 K to 300 K. [c]Determined by DSC analysis at the scanning rate of 5°C min^{-1}. [d]Curie constant. [e]Weiss temperature. [f]Transition from the N* phase to the crystalline phase occurred below 25°C

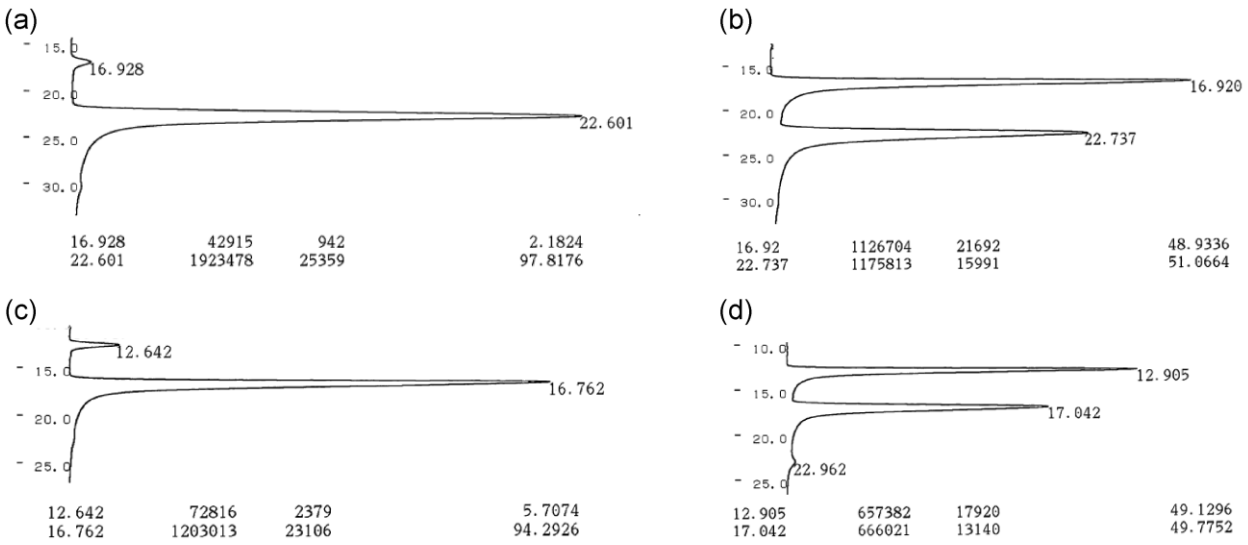

Fig. S1 HPLC chromatograms. (a) (2*S*,5*S*)-**2a** (96% *ee*), (b) (±)-**2a** , (c) (2*S*,5*S*)-**2b** (89% *ee*) and (d) (±)-**2b**.

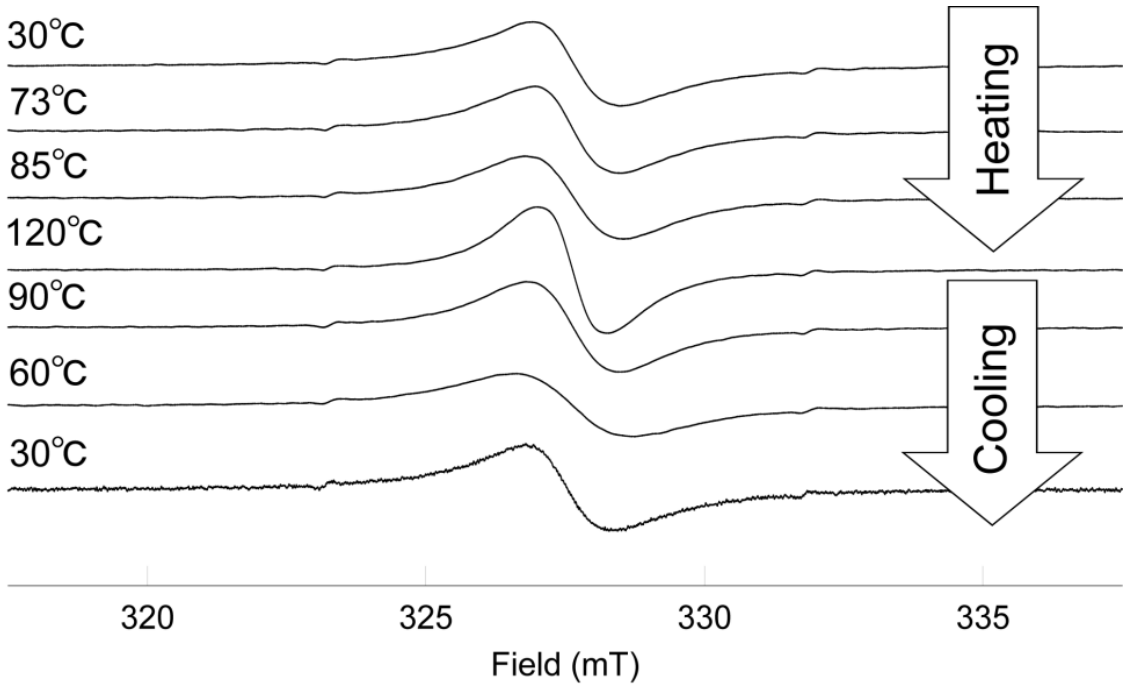

Fig. S2 Selected EPR spectra of (2*S*,5*S*)-**2a** (96% *ee*) measured at various temperatures from the crystalline phase (top) to the supercooled phase (bottom) through the LC and isotropic phases.

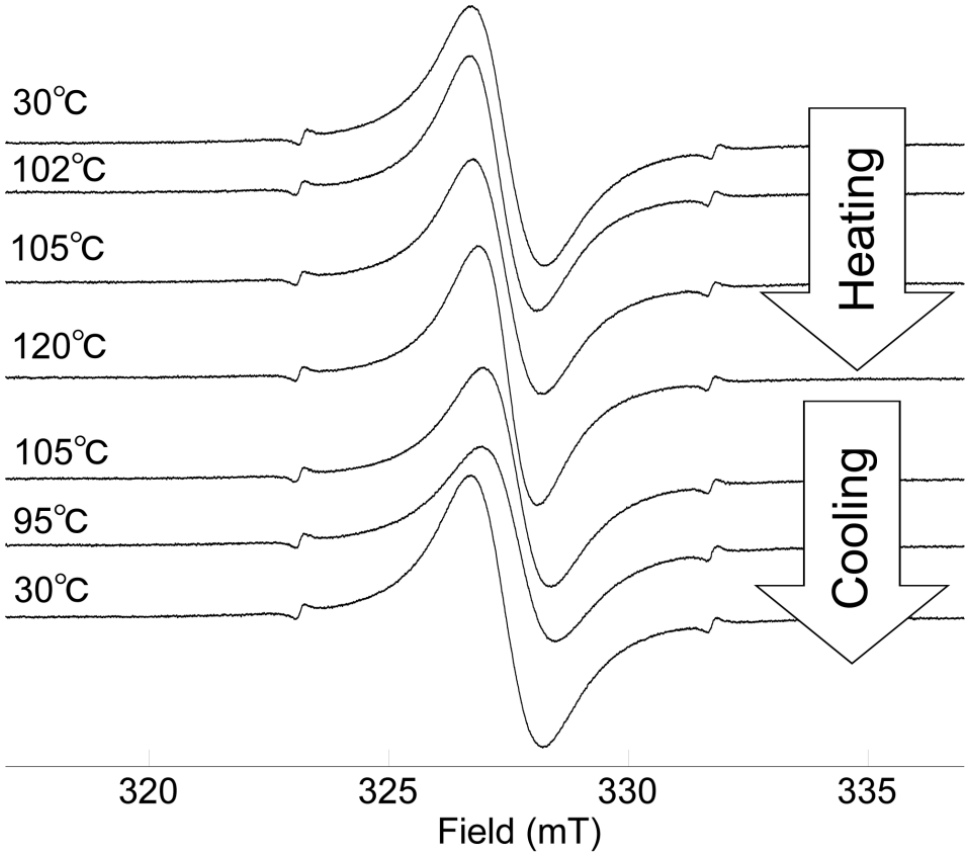

Fig. S3 Selected EPR spectra of (±)-**2a** measured at various temperatures from the crystalline phase (top) to the supercooled phase (bottom) through the LC and isotropic phases.

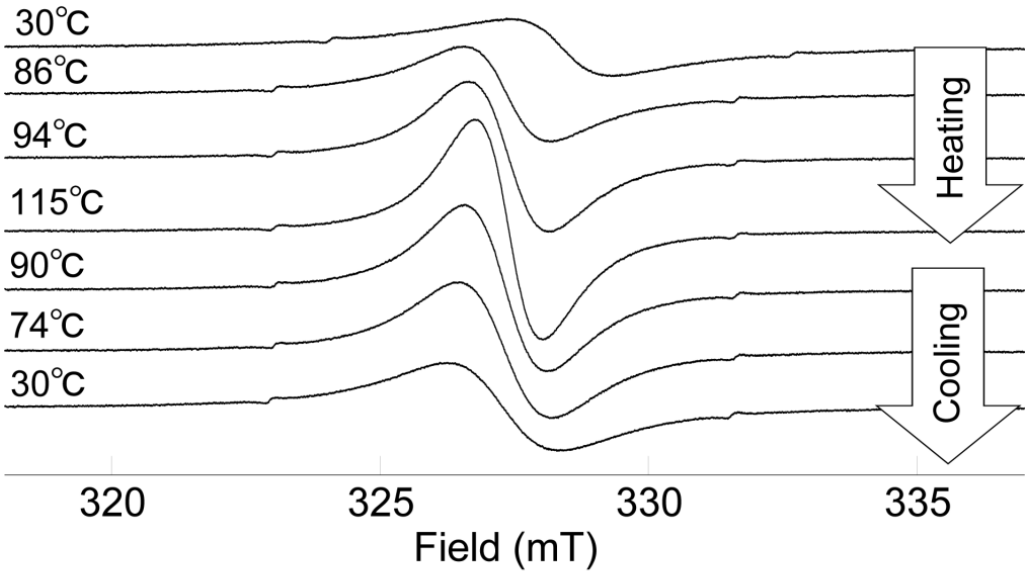

Fig. S4 Selected EPR spectra of (2*S*,5*S*)-**2b** (89% *ee*) measured at various temperatures from the crystalline phase (top) to the supercooled phase (bottom) through the LC and isotropic phases.

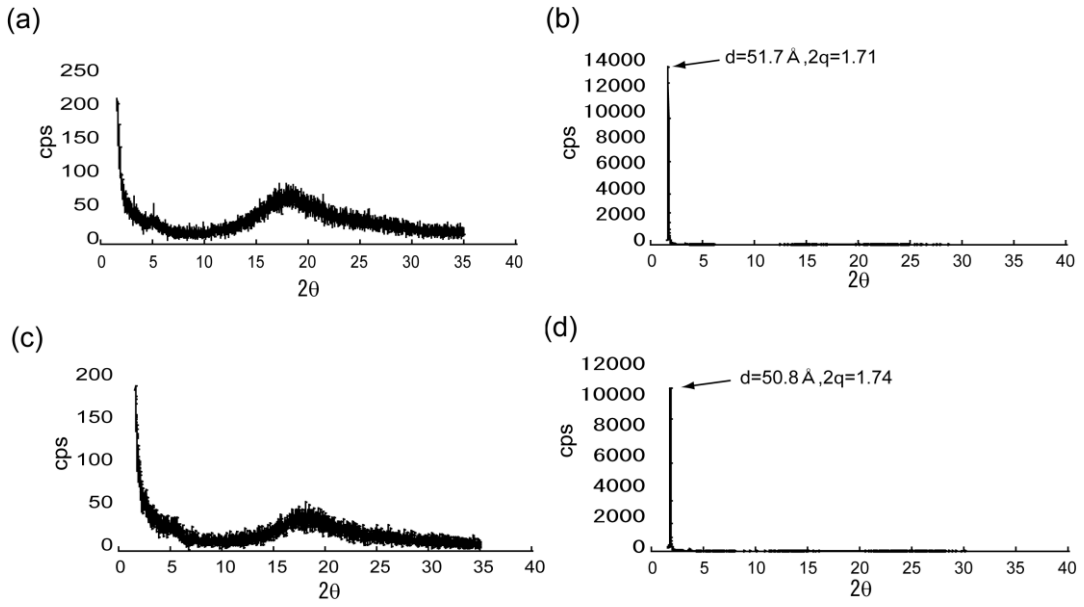

Fig. S5 XRD patterns of (a) (2*S*, 5*S*)-**2a** (96% *ee*) at 95°C, (b) (2*S*, 5*S*)-**2b** (89% *ee*) at 80°C (c) (±)-**2a** at 98°C and (d) (±)-**2b** at 98°C in the cooling run.

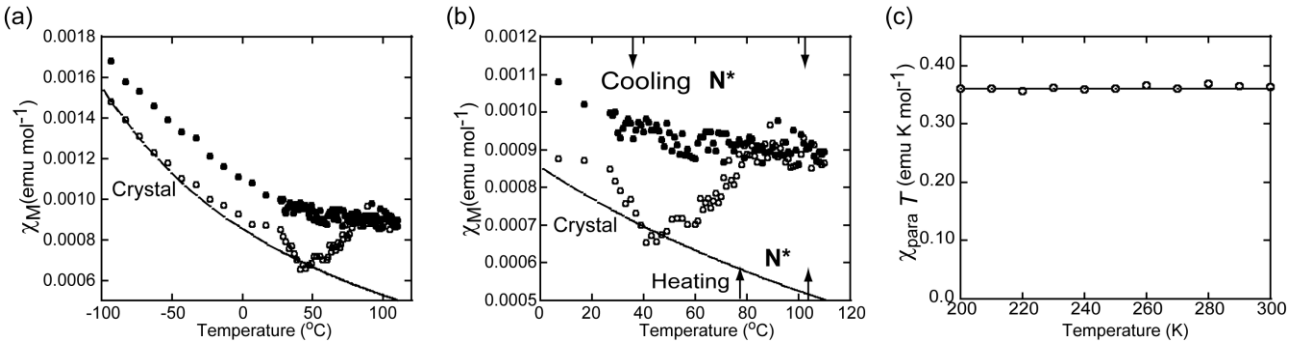

Fig. S6 Temperature dependence of molar magnetic susceptibility (χ_M) of (2*S*,5*S*)-**2a** (96% *ee*) at a field of 0.05 T in the temperature range of (a) -100°C to +120°C and (b) 0°C to +120°C. (c) $\chi_{para}T$-*T* plots of (2*S*,5*S*)-**2a** at a field of 0.5 T in the temperature range of 200 to 300 K. Open circles and filled circles represent the first heating and cooling runs, respectively. The Solid lines show Curie-Weiss fitting curves. The LC temperatures determined by differential scanning calorimetry at a scanning rate of 5°C min^{-1} upon the first heating and cooling processes are shown by the lower and upper allows inside the panel b, respectively.

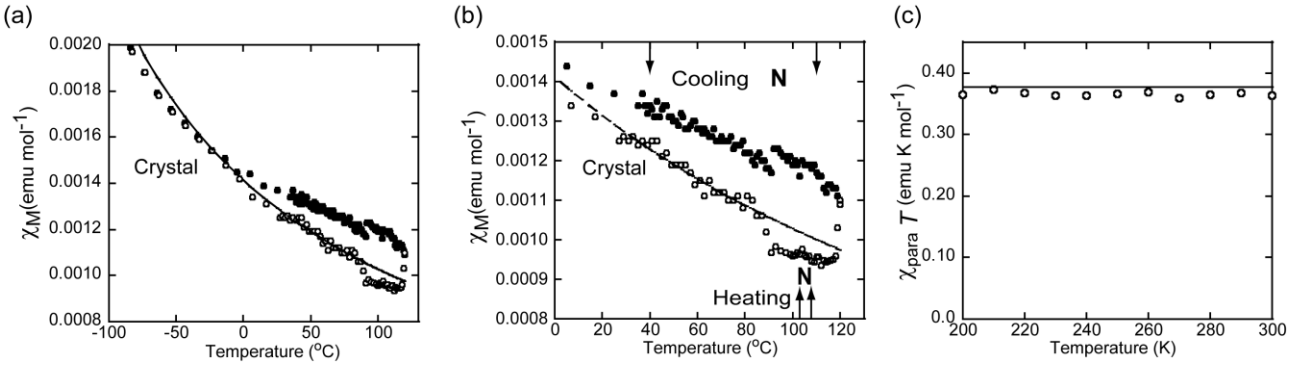

Fig. S7 Temperature dependence of molar magnetic susceptibility (χ_M) of (±)-**2a** at a field of 0.05 T in the temperature range of (a) -100°C to +130°C and (b) 0°C to +130°C. (c) $\chi_{para}T$-T plots of (±)-**2a** at a field of 0.5 T in the temperature range of 200 to 300 K. Open circles and filled circles represent the second heating and cooling runs, respectively. The Solid lines show Curie-Weiss fitting curves. The LC temperatures determined by differential scanning calorimetry at a scanning rate of 5°C min^{-1} upon the second heating and cooling processes are shown by the lower and upper allows inside the panel b, respectively.

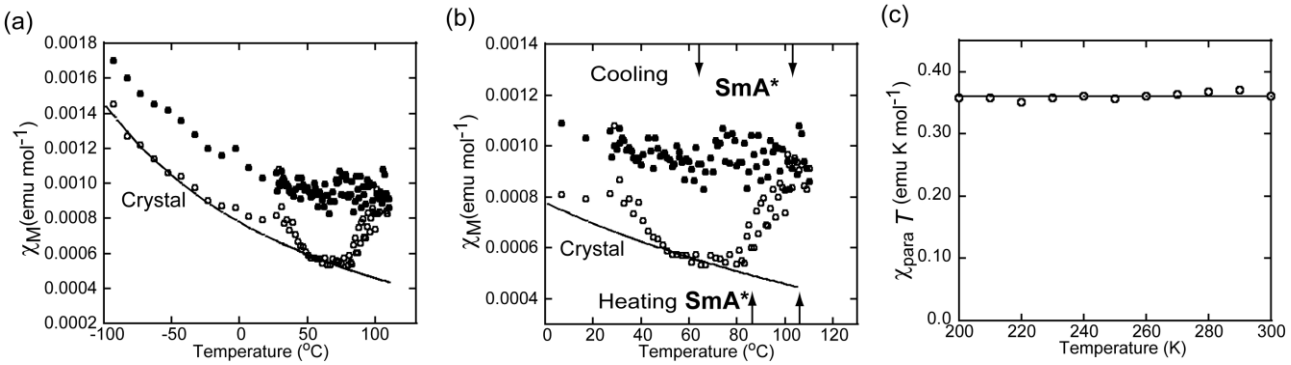

Fig. S8 Temperature dependence of molar magnetic susceptibility (χ_M) of (2*S*,5*S*)-**2b** (89% *ee*) at a field of 0.05T in the temperature range of (a) -100°C to +130°C and (b) 0°C to +130°C. (c) $\chi_{para}T$-T plots of (2*S*,5*S*)-**2b** at a field of 0.5 T in the temperature range of 200 to 300 K. Open circles and filled circles represent the first heating and cooling runs, respectively. The Solid lines show Curie-Weiss fitting curves. The LC temperatures determined by differential scanning calorimetry at a scanning rate of 5°C min^{-1} upon the first heating and cooling processes are shown by the lower and upper allows inside the panel b, respectively.

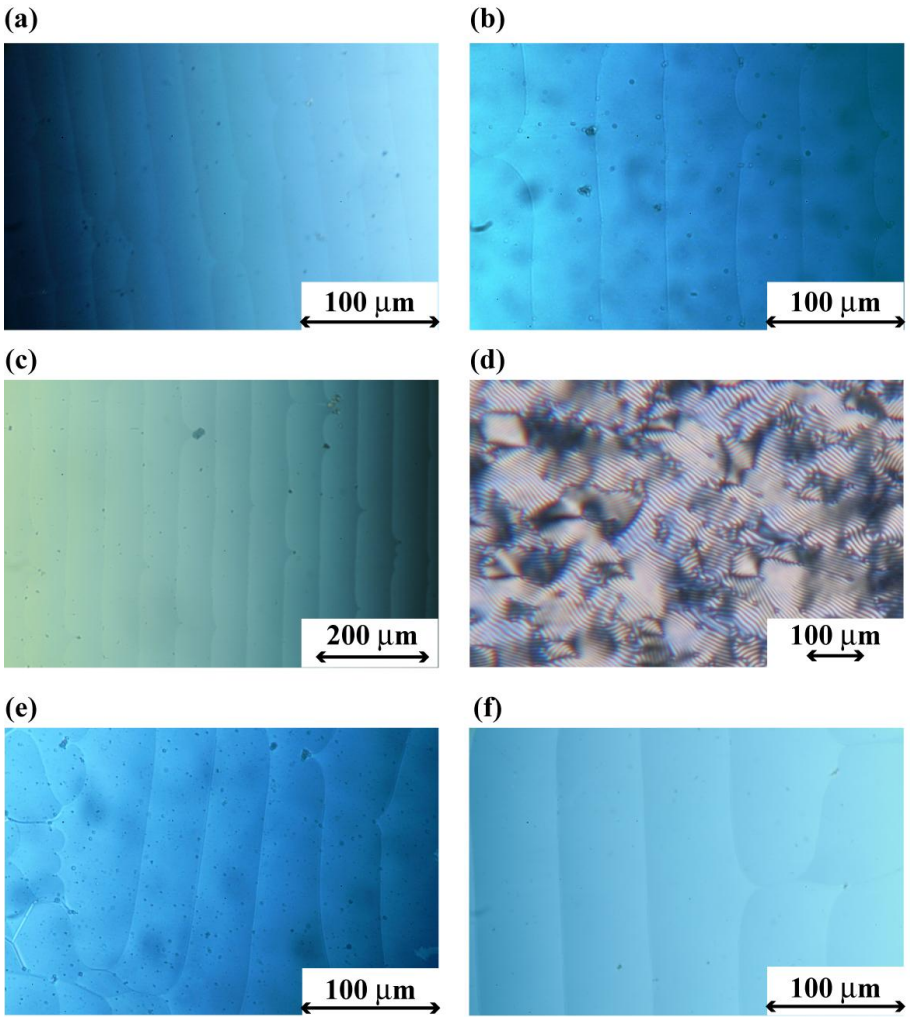

Fig. S9 Porlarized optical microphotographs of **2a** in the cooling run at 80 ºC. (a,b,c) Grandjean texture for N* phase of (2*S*,5*S*)-**2a** of 96% *ee*, 60% *ee*, and 40 % *ee*, respectively, in a wedge cell. (d) Finger print texture for N* phase of (±)-**2a** with 5 wt% of (-)-TADDOL under random conditions. e,f) Grandjean texture for N* phase of (±)-**2a** with 4.0 wt% of (*S*)-BICH and 2.5 wt% of (*S*)-BICH, respectively, in a wedge cell.

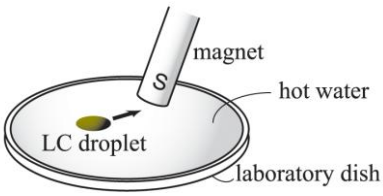

Fig. S10 Schematic representation of the motion of a magnetic LC droplet on water under the influence of a permanent magnet.

Information of Movies

Movie S1 Attraction by permanent magnet of the N* droplet of (2*S*,5*S*)-**2a** (96% *ee*) on water. The movie shows the attraction by a magnet (maximum 0.5T) of the LC droplet on water at 75°C in a thin laboratory dish (34 mm ϕ x 2 mm).

Movie S2 Attraction by permanent magnet of the partially crystallized N droplet of (±)-**2a** on water. The movie shows the slow attraction by a magnet (maximum 0.5T) of the LC droplet on water at 75°C in a thin laboratory dish (34 mm ϕ x 2 mm).

Movie S3 Attraction by permanent magnet of the SmA* droplet of (2*S*,5*S*)-**2b** (89% *ee*) on water. The movie shows the attraction by a magnet (maximum 0.5T) of the LC droplet of on water at 75°C in a thin laboratory dish (34 mm ϕ x 2 mm).